RSC Advances

PAPER

View Article Online
View Journal | View Issue

Cite this: *RSC Adv.*, 2015, **5**, 81362

Efficient absorption of ammonia with hydroxyl-functionalized ionic liquids†

Zhijie Li,[ab] Xiangping Zhang,*[a] Haifeng Dong,[a] Xiaochun Zhang,[a] Hongshuai Gao,[a] Suojiang Zhang,*[a] Jianwei Li[b] and Congmin Wang[c]

Ammonia (NH_3) emitted from the ammonia synthesis process is a kind of waste chemical resource and a major environmental pollutant. The traditional water scrubbing method suffers from high energy consumption due to the concentrated NH_3 from aqueous ammonia. Therefore, it is desirable to develop novel absorbents for the efficient, reversible and environmentally-friendly recovery of NH_3. In this paper, a series of hydroxyl-functionalized imidazolium ILs ([EtOHmim]X, X = $[NTf_2]$, $[PF_6]$, $[BF_4]$, [DCA], [SCN] and $[NO_3]$) were designed and prepared. Their physical properties and NH_3 absorption capacities under different temperatures and pressures were systematically investigated. The effects of hydroxyl cation, anionic structures, pressure and temperature on absorption performance were sufficiently studied. In addition, the absorption mechanism was investigated in detail by spectral analysis and quantum chemistry calculations. Compared with conventional IL [Emim]X, a higher absorption capacity was achieved by introducing the hydroxyl group on the imidazolium cation. The mechanism results showed the fascinating absorption performance of the task-specific ILs was attributed to the stronger hydrogen bonding interaction between NH_3 and the H atom of the hydroxyl group. Considering the excellent absorption performance, high thermal stability, and super reversibility, this type of IL provides great improvement over conventional IL and shows their enormous potential in NH_3 recovery.

Received 13th July 2015
Accepted 16th September 2015

DOI: 10.1039/c5ra13730f

www.rsc.org/advances

1. Introduction

As a typical environmental pollutant, the increase of ammonia (NH_3) release is leading to different environmental problems including eutrophication of ecosystems and the formation of fine particulate matter[1] and seriously threatens human health. Meanwhile, NH_3 is one of the important chemical raw materials and widely applied in producing nitric acid, nitrogenous fertilizer and so on. Therefore, removal and recovery of NH_3 is of great significance. Up to now, water scrubbing has been the most common method due to its high NH_3 absorption capacity. However, this method suffers from several inherent drawbacks such as high energy consumption, large amounts of waste water and difficult reclamation of NH_3. Hence, it is desirable to develop environmentally-friendly, recyclable absorbents for efficient NH_3 absorption.

It is increasing recognized that ionic liquids (ILs) are promising absorbents because of their special properties such as negligible vapor pressure, wide liquid temperature range, high thermal stability[2] and adjustability[3] and have been paid great attentions on separation of CO_2,[4–11] SO_2 [12–19] and H_2S.[6,20–23] On the contrast, the reports on NH_3 absorption by ionic liquids are scare. In fact, the results reported have shown that ionic liquids have great potential for NH_3 absorption. Yokozeki *et al.*[24,25] demonstrated the conventional ionic liquids such as $[Bmim][PF_6]$, [Hmim][Cl] had high NH_3 absorption performance and the anion had little effect on NH_3 solubility. Li *et al.*[26] reported NH_3 solubility increased when the length of cation's alkyl increased. Shi *et al.*[27] testified the cation played the leading role in determining NH_3 solubility and they found a strong hydrogen bonding could be formed between NH_3 molecule and the ring H atom of the [Emim] cation by molecular simulation.

Although great efforts had been made to improve the NH_3 absorption, the solubility of NH_3 in these conventional ILs was relatively low. What is more, the research on the mechanism of IL–NH_3 system was very scanty and not comprehensive. Shi *et al.*[27] investigated the NH_3 absorption mechanism just by molecular simulation. As reported, hydrogen bonding interaction between IL and NH_3 was beneficial to enhance solubility,[28] thus in this work, hydroxyl, as the hydrogen bonding donor group, was introduced into the imidazolium cation for further improving the absorption. NH_3 absorption capacities of these hydroxyl-functionalized ILs at different temperatures and

[a]*Beijing Key Laboratory of Ionic Liquids Clean Process, State Key Laboratory of Multiphase Complex Systems, Institute of Process Engineering, Chinese Academy of Sciences, Beijing, 100190, China. E-mail: xpzhang@home.ipe.ac.cn*

[b]*State Key Laboratory of Chemical Resource Engineering, Beijing University of Chemical Technology, Beijing, 100029, China*

[c]*Department of Chemistry, Zhejiang University, Hangzhou, 310027, China*

† Electronic supplementary information (ESI) available. See DOI: 10.1039/c5ra13730f

pressures were systematically investigated. Furthermore, the absorption mechanism was deeply explored by experimental spectra analysis and quantum chemistry calculations.

2. Experimental section

2.1. Materials

NH_3 (99.999%) was supplied by Beijing Beiwen Gas Factory. 1-Methylimidazole (99.0%), $NaBF_4$ (98.0%), $LiNTf_2$ (98.5%) and NaSCN (98.5%) were purchased from Sinopharm Chemical Reagent Co., Ltd. 2-Chloroethanol (99.0%) was purchased from Xiya Chemical Co., Ltd. KPF_6 (98.0%) and $NaNO_3$ (99.0%) were purchased from Beijing Chemical Works Co., Ltd. All the chemicals above were used without further purification. 1-Ethyl-3-methylimidazolium chloride was obtained from Linzhou Keneng Materials Technology Co., Ltd. 1-2(-Hydroxyethyl)-3-methylimidazolium salt [EtOHmim]X and 1-ethyl-3-methylimidazolium salt [Emim]X were synthesized in our laboratory.

2.2. Synthesis of ionic liquids

$[EtOHmim][NTf_2]$ was synthesized by the method shown in Scheme S1 (seeing ESI†) according to the literature.[29] Preparation of [EtOHmim][Cl]: 1-methylimidazole (41.00 g, 0.5 mol) was put in a round-bottom flask (250 mL) and 2-chloroethanol (48.31 g, 0.6 mol) was added slowly. The mixture was stirred for 24 hours at 353.15 K. Then the product was washed several times with ethyl acetate. The [EtOHmim][Cl] white solid was obtained after filtration and vacuum drying for 48 hours at 343.15 K. Preparation of $[EtOHmim][NTf_2]$: [EtOHmim][Cl] (16.252 g, 0.1 mol) and $LiNTf_2$ (28.69 g, 0.1 mol) were mixed and some water was added as solvent. Then the mixture was stirred for 24 hours at ambient temperature. By separating the mixture, the supernate was removed and ionic liquid was washed by deionized water for several times until there was no sediment formed when $AgNO_3$ was added in water. At last, high-purity $[EtOHmim][NTf_2]$ was obtained after rotary evaporation and vacuum drying at 373.15 K for 64 hours. The synthesis methods of other ILs [EtOHmim]X (X = $[PF_6]^-$, $[BF_4]^-$, $[DCA]^-$, $[SCN]^-$, $[NO_3]^-$) and [Emim]X (X = $[NTf_2]^-$, $[BF_4]^-$, $[NO_3]^-$) were similar to that of $[EtOHmim][NTf_2]$ except the solvent was replaced by acetone. The different structures of [EtOHmim] cation and [Emim] cation were presented in Fig. 1.

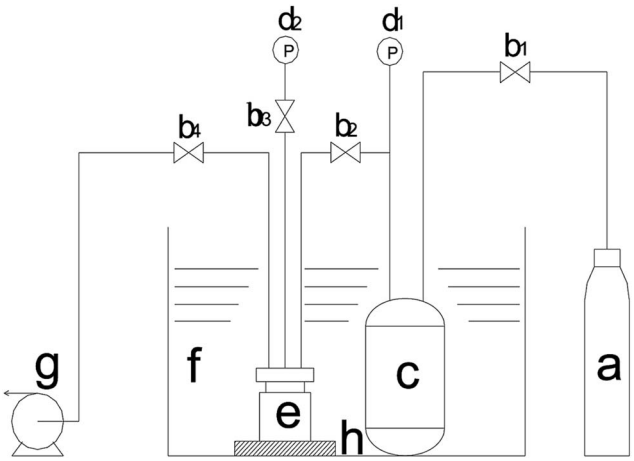

Fig. 2 Schematic diagram of NH_3 absorption apparatus. (a) NH_3 cylinder; (b_1–b_4) valve; (c) storage tank; (d_1 and d_2) pressure sensor; (e) absorption vessel; (f) thermostatic bath; (g) vacuum pump; (h) magnetic stirrer.

2.3. Characterization and physical properties

^1H NMR and ^{13}C NMR spectra were recorded on a Bruker spectrometer (600 Hz) in deuterated dimethyl sulfoxide (DMSO-d_6) with tetramethylsilane as the internal standard. The NMR data of ILs were presented in ESI.† FT-IR spectra were obtained in the range of 400–4000 cm^{-1} on a Thermo Nicolet 380 spectrometer. The water contents of the ILs were measured by Karl Fisher coulometers C20 and had been reduced less than 400 ppm. The chlorine contents were tested by ioniza chlorine analyzer (Leici PXSJ-226). The densities of ionic liquids were measured by a density meter (Anton Paar DMA 5000) with an accuracy of ± 0.000005 g cm^{-3}. The viscosities were measured by an automated micro viscometer (Anton Paar AMVn). The thermal decomposition temperatures were tested by TGA (Q5000 V3.15 Build 263) from room temperature to 773.15 K with a heating rate of 10 K min^{-1} under N_2 atmosphere. The glass transition temperatures were measured on a Mettler Toledo DSC1 between 123.15 and 298.15 K at a heating rate of 10 K min^{-1} under N_2 atmosphere.

2.4. Apparatus and procedures

NH_3 solubility was measured by the gas–liquid equilibrium apparatus (shown in Fig. 2) which was similar to that in our previous work.[17,30] In a typical experiment, the temperature was

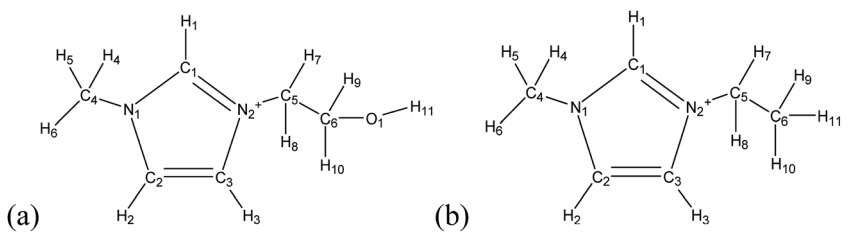

Fig. 1 Schematics of $[EtOHmim]^+$ (a) and $[Emim]^+$ (b), with atom labels.

fixed by a thermostatic water bath with an uncertainty of ±0.1 K and the pressure was measured by pressure transmitters with an accuracy of 0.0001 kPa. About 5.0 g IL was placed into the absorption vessel (30 mL), then the gas in absorption vessel was removed by vacuum pump. The NH_3 in storage tank (500 mL) was charged into the absorption vessel slowly through the valve (b_2). Then the magnetic stirrer was opened to enhance the dissolution. It is supposed the equilibrium is reached after the pressure keeps unchanged for 30 min. The solubility of NH_3 was calculated by Peng–Robinson (P–R) eqn (1) through the pressure variation in storage tank and absorption vessel:

$$p = \frac{RT}{V_m - b} - \frac{a}{V_m(V_m + b) + b(V_m - b)} \quad (1)$$

$$a = a_c\alpha \quad (1.1)$$

$$a_c = 0.457235\frac{(RT_c)^2}{p_c} \quad (1.2)$$

$$b = 0.077796\frac{RT_c}{p_c} \quad (1.3)$$

$$\alpha^{0.5} = 1 + (0.37464 + 1.54226\omega - 0.26992\omega^2)(1 - T_r^{0.5}) \quad (1.4)$$

$$T_r = \frac{T}{T_c} \quad (1.5)$$

$$n_{NH_3} = \Delta\left(\frac{V_S}{V_{m,s}}\right) - \left(\frac{V_A - V_{IL}}{V_{m,A}}\right) \quad (2)$$

$$x_{NH_3} = \frac{n_{NH_3}}{n_{NH_3} + n_{IL}} \quad (3)$$

where p, V_m and T are denoted to pressure, molar volume and temperature, respectively. R is the gas constant and a, b, a_c, α are the parameters of the cubic equation. T_c is the critical temperature, p_c is the critical pressure and T_r is relative temperature. n_{NH_3} is the amount of NH_3 absorbed and n_{IL} is the amount of ionic liquid. V_S, V_A and V_{IL} represent the volumes of storage tank, absorption vessel and ionic liquid, respectively. $V_{m,S}$ and $V_{m,A}$ are the molar volume of storage tank and absorption vessel. x_{NH_3} represents the mole fraction of NH_3 absorbed.

2.5. Thermodynamic analysis

Henry's constant (k_H) is an important parameter to present the absorption behavior of NH_3 in ILs. The Henry's constants of NH_3 absorbed in ionic liquids at different temperatures could be obtained by the following eqn (4) and the fugacity coefficient (φ) was calculated according to the P–R equation. Subsequently, the changes of standard Gibbs free energy ($\Delta_{sol}G^\theta$), standard enthalpy ($\Delta_{sol}H^\theta$) and standard entropy ($\Delta_{sol}S^\theta$) could be estimated by the following eqn (6)–(8).

$$k_H(T) = \lim_{p\to 0}\left[\frac{f_1(T,p)}{x_1}\right] = \frac{p^{eq}\varphi_1(T,p)}{x_1} \quad (4)$$

$$\ln\varphi = \frac{pV}{RT} - 1 - \ln\frac{p(V-b)}{RT} - \frac{\alpha}{2^{1.5}bRT}\ln\frac{V + (\sqrt{2}+1)b}{V - (\sqrt{2}-1)b} \quad (5)$$

$$\Delta_{sol}G^\theta = RT\ln(k_H/p^\theta) \quad (6)$$

$$\Delta_{sol}H^\theta = -RT^2\frac{\partial\ln(k_H/p^\theta)}{\partial T} \quad (7)$$

$$\Delta_{sol}S^\theta = \frac{\Delta_{sol}H^\theta - \Delta_{sol}G^\theta}{T} \quad (8)$$

where $f_1(T, p)$ represents the fugacity of NH_3 and $\varphi_1(T, p)$ is the fugacity coefficient of NH_3 solute in the gas phase. p^{eq} is the equilibrium partial pressure of NH_3 and p^θ represents the standard pressure.

3. Results and discussion

3.1. Physical properties of ILs

Density and viscosity of IL were fundamental properties for gas separation process, hence these properties were measured at different temperatures from 298.15 K to 343.15 K. Fig. 3 shows the densities of the functionalized ILs decrease linearly with the increasing of temperature and they fall in the range from 1.15 to 1.58 g cm^{-1}. It can be found the densities are greatly affected by the different anions and [EtOHmim][DCA] shows the lowest density.

Fig. 4 shows the viscosities of the functionalized ILs with different anions range from 19.10 to 609.98 mPa s and decrease in an exponential manner with the increasing of temperature, which is in agreement with the other imidazolium ILs.[31] Viscosity activation energy (E_a) of IL is estimated by a fitting of the measured viscosity to Arrhenius expression[32] using the following equation:

$$\eta = \eta_\infty \exp(-E_a/RT) \quad (9)$$

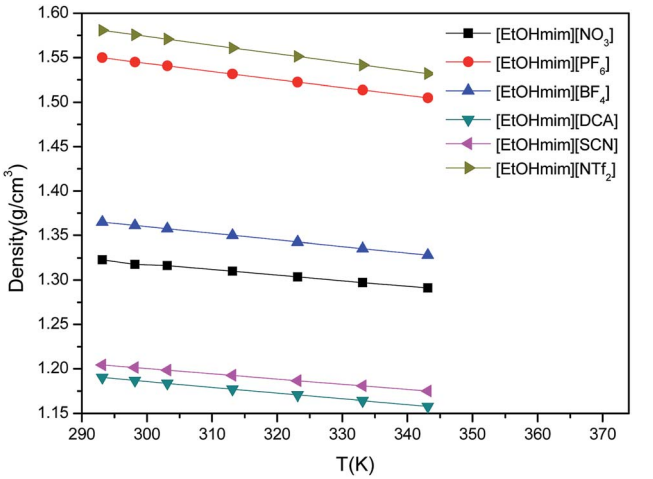

Fig. 3 Densities of task-specific ILs at different temperatures.

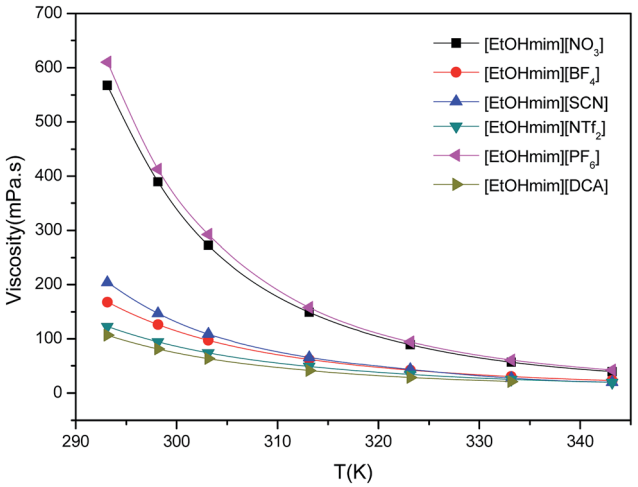

Fig. 4 Viscosities of task-specific ILs at different temperatures.

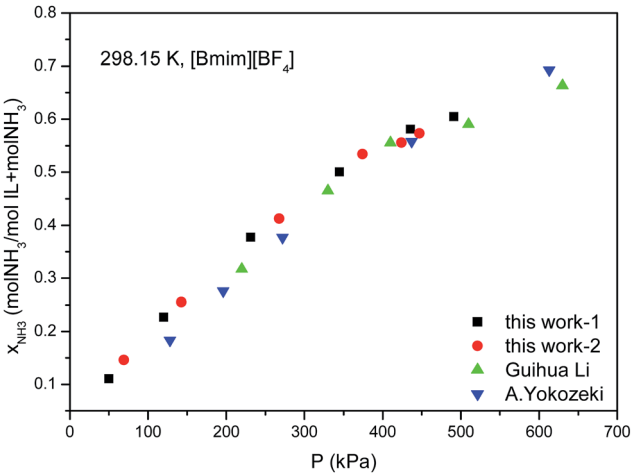

Fig. 5 NH_3 absorption capacity of [Bmim][BF_4] in this work and the literatures[25,26] at 298.15 K.

In this equation, η is the viscosity at any temperature and η_∞ is the apparent viscosity at infinite temperature. The values of E_a for [EtOHmim]X shown in Table S1† and they range from 31 to 45 kJ mol^{-1}. Generally, the larger value will indicate the higher viscosity. The calculated viscosity activation energies of the task-specific ILs are larger than those of the typical solutions ($E_{a\ water}$ = 17.0 kJ mol^{-1}, $E_{a\ benzene}$ = 10.4 kJ mol^{-1}, and $E_{a\ acetone}$ = 7.1 kJ mol^{-1}).[33] Although [EtOHmim][DCA] shows the lowest viscosity, the introducing of hydroxyl group results in the larger viscosity than that of [Emim][DCA] (18.4 kJ mol^{-1}), which indicates that cations also influence the viscosity.

In addition, thermal stability of IL is also very significant for gas separation, because high thermal stability is beneficial for reversible absorption and desorption. The TGA curves are shown in Fig. S2† and the results of DSC and TGA are summarized in Table 1. The thermal decomposition temperatures (T_d) of the six functionalized ILs are all above 500 K and [EtOHmim][NTf_2] shows the highest decomposition temperature. Pablo's group reported the T_d of [Emim][SCN] was 538.6 K,[34] which was similar to that of [EtOHmim][SCN]. It shows the introducing of hydroxyl is almost no influence on the thermal stability.

3.2. NH_3 absorption performance of [EtOHmim]X

First, NH_3 absorption capacity of [Bmim][BF_4] was investigated at 298.15 K and compared with the values reported from the available literatures in order to validate the reliability of data in this work. Fig. 5 shows the solubility is similar to that in literatures,[25,26] which indicates that the experiment apparatus is reliable and the data is credible. Then, a series of vapor liquid equilibrium measurements were performed at pressures from 0 to 0.6 MPa (A (absolute)) and temperatures from 298.15 to 343.15 K. The solubility data of pressure–temperature–composition (p–T–x) of the task-specific ILs are presented in ESI Table S2.†

3.2.1 Effect of hydroxyl group cation. To assess the effect of hydroxyl group cation on NH_3 solubility, the absorption capacity of functionalized ILs [EtOHmim]X were compared with that of conventional ILs [Emim]X at 333.15 K. The results show that the former captures higher amount of NH_3. Fig. 6 shows that when the anion is same, an obvious increase of solubility is found in [EtOHmim]X. For example, at 102.7 kPa, the solubility of [EtOHmim][BF_4] is 0.27 in mole fraction, and at 547.0 kPa, the mole fraction is 0.56. For [Emim][BF_4], the solubility at

Table 1 The melting points (T_m), glass transition temperatures (T_g) and the thermal decomposition temperatures (T_d) of the functionalized ILs

[EtOHmim]X	T_m (K)	T_g (K)	T_d (K)
[NTf_2]	—	190.02	643.75
[PF_6]	308.32	187.67	564.11
[BF_4]	—	187.98	542.81
[DCA]	—	185.28	507.18
[SCN]	286.32	185.64	543.91
[NO_3]	281.32	183.35	546.42

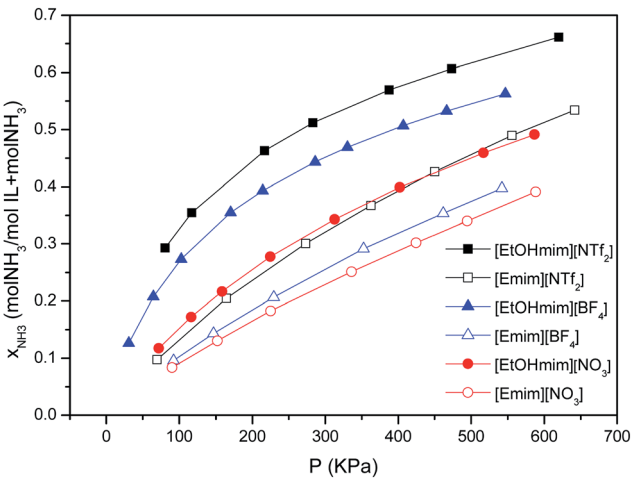

Fig. 6 Comparison of NH_3 solubilities in [EtOHmim]X and [Emim]X (X = $[NTf_2]^-$, $[BF_4]^-$, $[NO_3]^-$) at 333.15 K.

103.1 kPa is 0.10 and at 548.2 kPa the mole fraction is 0.40. It suggests that the absorption capacities of imidazolium ILs are distinctly enhanced due to the introducing of hydroxyl group. A possible explanation is that hydrogen bonding interaction brings about the improved absorption performance. The acid hydroxyl, regarded as the hydrogen bonding donor group, could form stronger hydrogen bonding with the N atom of NH_3 than the conventional [Emim]X. In addition, because the viscosities of [EtOHmim]X are slightly larger than [Emim]X due to the introducing of hydroxyl group, the equilibrium time for NH_3 absorption in [EtOHmim][NTf_2] and [Emim][NTf_2] have been also measured respectively using the same apparatus. The variations of pressure with time are shown in Fig. S3.† We can find the equilibrium time of [EtOHmim][NTf_2] (about 6 min) is slightly longer than [Emim][NTf_2] (about 4 min). In conclusion, hydroxyl-functionalized ILs may be more suitable to be the solvents for NH_3 recovery than conventional ILs.

3.2.2 Effect of anions. With the comparison of NH_3 solubilities in ILs with different anions, it is observed that anions also have an obviously effect on NH_3 absorption. Fig. 7 presents the ILs of anions containing fluoride ($[NTf_2]^-$, $[PF_6]^-$, $[BF_4]^-$) have higher solubility than others ($[DCA]^-$, $[SCN]^-$, $[NO_3]^-$). The absorption capacities of these ILs decrease in the following order: $[NTf_2]^- > [PF_6]^- > [BF_4]^- > [SCN]^- > [NO_3]^-$. Especially, for [DCA] anion, when the pressure is less than 150 kPa, its absorption capacity is lower than that of $[NO_3]^-$; but when the pressure is between 150 to 400 kPa, its absorption capacity falls in that between $[SCN]^-$ and $[NO_3]^-$. The similar conclusion can be obtained at other temperatures. The reason for the higher absorption capacities of ILs containing fluoride may be that the F atom of the anions can also form hydrogen bonding interaction with the H atom of NH_3.[27] From a molecular perspective, there are three hydrogen bonding donors on NH_3, four acceptors on [BF_4], six acceptors on [PF_6] and 10 acceptors on [NTf_2]. Therefore, the relatively stronger hydrogen bonding interaction may be formed between the H atom of NH_3 and [NTf_2] anion, which is consistent with the highest solubility of [EtOHmim][NTf_2]. Because of the highest absorption capacity of [EtOHmim][NTf_2], this ionic liquid is investigated as a typical example.

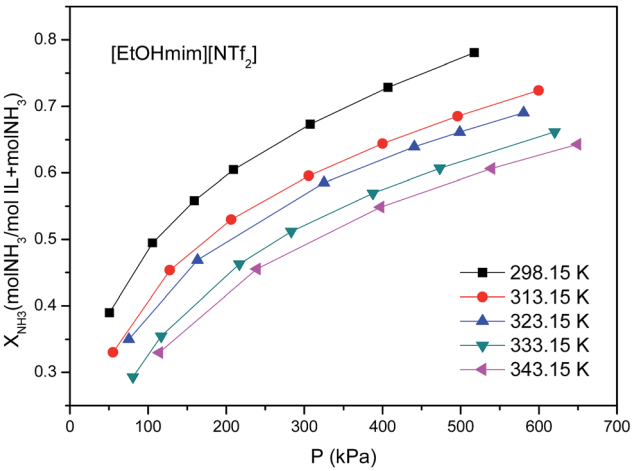

Fig. 8 The solubilities of NH_3 in [EtOHmim][NTf_2] at different temperatures.

3.2.3 Effects of temperature and pressure. The effects of temperature and pressure on NH_3 absorption in [EtOHmim][NTf_2] are displayed in Fig. 8. It can be seen that with the increasing of temperature, the absorption capacity of hydroxyl-functionalized ILs dramatically decreases. Besides, the molar fraction of NH_3 increases continuously with the increasing of pressure. It suggests that low temperature is better for NH_3 absorption and the desorption can be carried out at high temperature, which is in good agreement with the literature.[24]

3.3. Desorption and recycling

Recyclability is another important factor to evaluate an ionic liquid solvent and a key issue for potential industrial application, thus the absorption cycles of [EtOHmim][NTf_2] have

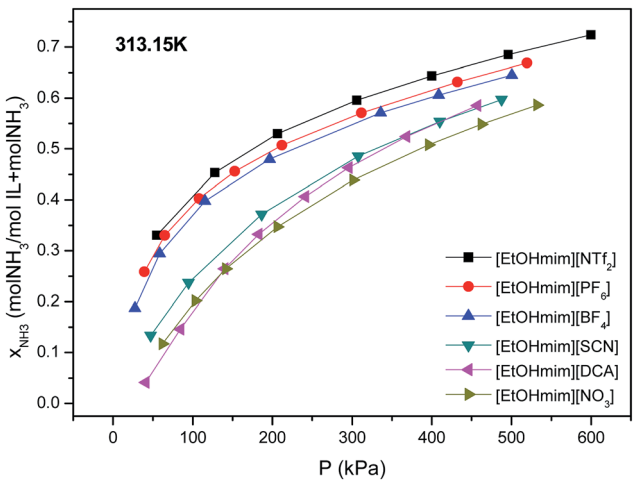

Fig. 7 The solubilities of NH_3 in task-specific ILs with different anions at 313.15 K.

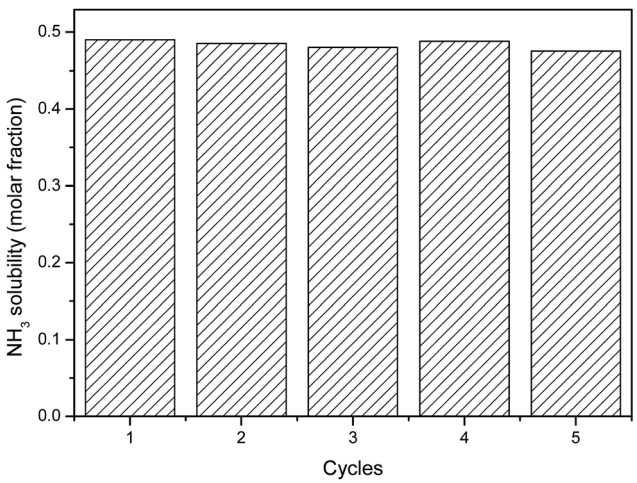

Fig. 9 Recycling of [EtOHmim][NTf_2] for NH_3 absorption at 298.15 K and 100 kPa.

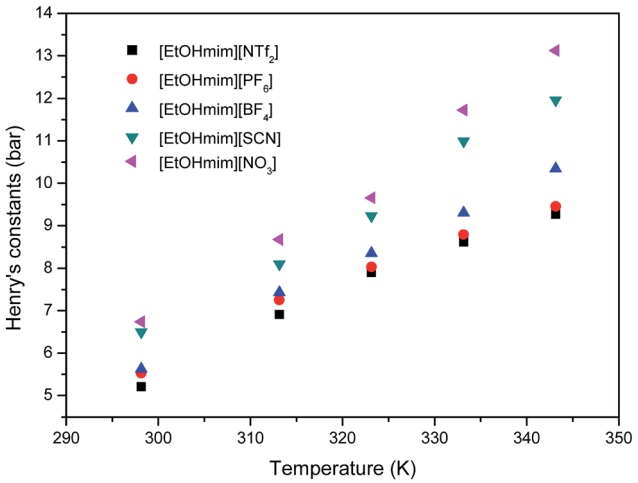

Fig. 10 Henry's constants of NH_3 in task-specific ILs *versus* temperature.

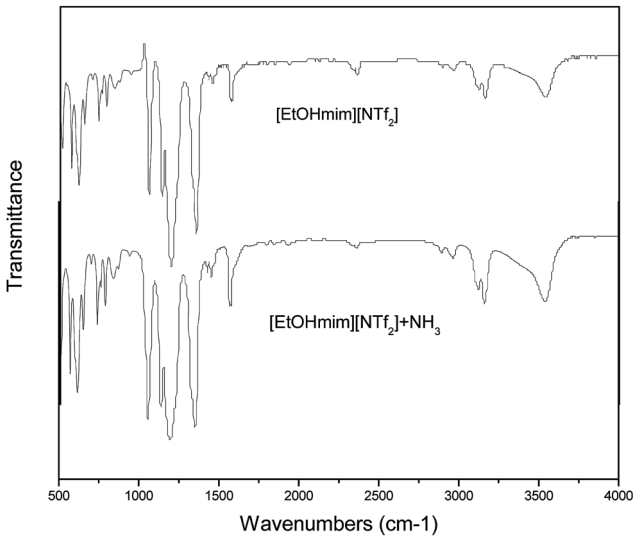

Fig. 11 FT-IR spectra of [EtOHmim][NTf_2] before and after absorption of NH_3.

been measured at 298.15 K and 100 kPa. First, the solubility was investigated in the fresh IL, then NH_3-saturated IL was desorbed under a vacuum of 0.15 kPa for 1 hour at 353.15 K and reused for NH_3 absorption. The absorption–desorption experiments were performed for five cycles. Fig. 9 shows that the solubility keeps almost unchanged after five cycles. It is revealed that [EtOHmim][NTf_2] can be reused with almost same capacity, which suggests the functionalized ILs have good recyclability.

3.4. Thermodynamic properties of NH_3 in ILs

Henry's constants were calculated according to the solubility of NH_3. In Fig. 10, with the increasing of temperature, Henry's constants increase for each ionic liquid. The Henry's constants in the ILs containing fluoride are smaller than those of others, which accords with the higher NH_3 absorption capacity of the ILs containing fluoride. Thermodynamic parameters including standard enthalpy, standard Gibbs free energy, and standard entropy were also calculated and the results were presented in Table 2. Solution entropy represents the direction of disorder in the absorption process. Table 2 shows standard Gibbs free energy changes are positive and entropy changes are negative. Namely, at standard pressure, ammonia solution in [EtOHmim]X is a process of entropy decreasing. The value of ΔG increases with the increasing of temperature, which means higher temperature is unfavorable for NH_3 absorption. This conclusion is consistent with the experimental results. Solution enthalpy is an important parameter to evaluate the gas–liquid interaction.

Table 2 Thermodynamic parameters of NH_3 in [EtOHmim]X

T (K)	[EtOHmim][NTf_2]	[EtOHmim][PF_6]	[EtOHmim][BF_4]	[EtOHmim][SCN]	[EtOHmim][NO_3]
$\Delta_{sol}G^0$ (kJ mol^{-1})					
298.15	4.09	4.24	4.28	4.64	4.73
313.15	5.03	5.16	5.22	5.45	5.62
323.15	5.55	5.60	5.70	5.97	6.09
333.15	5.97	6.02	6.18	6.64	6.82
343.15	6.35	6.41	6.67	7.08	7.34
$\Delta_{sol}H^0$ (kJ mol^{-1})					
298.15	−9.39	−9.46	−9.83	−10.27	−11.01
313.15	−10.35	−10.44	−10.84	−11.33	−12.15
323.15	−11.03	−11.11	−11.55	−12.07	−12.94
333.15	−11.72	−11.81	−12.27	−12.83	−13.75
343.15	−12.43	−12.53	−13.02	−13.61	−14.59
$\Delta_{sol}S^0$ (J mol^{-1}K^{-1})					
298.15	−45.21	−45.94	−47.33	−50.02	−52.80
313.15	−49.14	−49.80	−51.30	−53.58	−56.75
323.15	−51.31	−51.72	−53.39	−55.82	−58.88
333.15	−53.09	−53.52	−55.38	−58.43	−61.74
343.15	−54.75	−55.20	−57.37	−60.29	−63.91

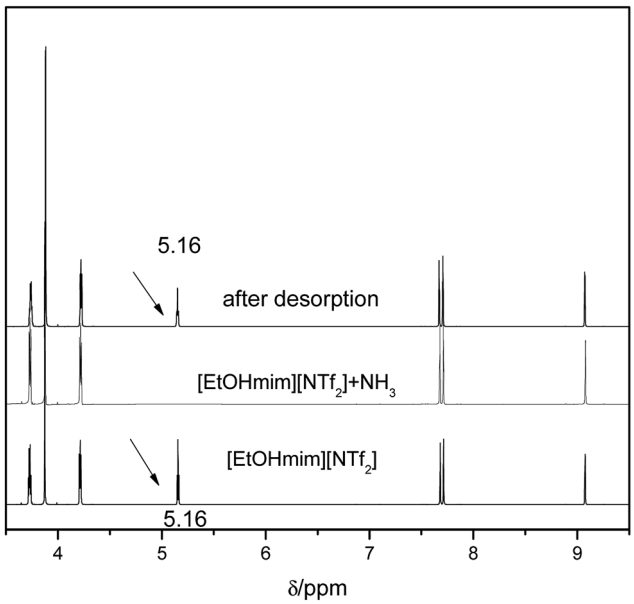

Fig. 12 ^{1}H NMR spectra of [EtOHmim][NTf_2] before and after NH_3 absorption.

From Table 2, the enthalpy changes are negative, which indicates the solution at standard pressure is exothermal. And this conclusion corresponds with the ordinary solution rules for most gas. The enthalpy changes increases with the increasing of temperature, it demonstrates the heat release in this solution process decreases with the increasing of temperature. Usually, a higher value of enthalpy signifies a stronger gas–liquid interaction. But for [EtOHmim]X, the order of solubility is not as same as that of enthalpy. For example, the solubility of [EtOHmim][NTf_2] is significantly higher than [EtOHmim][NO_3], but the absolute value of enthalpy in [EtOHmim][NO_3]–NH_3 system is higher than that in [EtOHmim][NTf_2]–NH_3 system. Therefore, for the ionic liquids with different anions, not only the interaction between NH_3 and ILs but also the free volume of anions plays important influence on solubility.

3.5. Mechanism of NH_3 absorption

The mechanism of NH_3 absorption was investigated by the comparison of FT-IR and ^{1}H NMR spectra of [EtOHmim]X before and after NH_3 absorption. Fig. 11 shows that there is no obvious change of FT-IR spectra for [EtOHmim][NTf_2] before and after NH_3 absorption. Furthermore, *in situ* FT-IR (shown in Fig. S4†) is applied to monitor the spectral variation of NH_3 absorption process for one hour, which also shows no distinct changes. Considering the absorption performance, the easy desorption behavior and no formation of new functional group, a possible explanation is that these novel ionic liquids absorb NH_3 through hydrogen bonding interaction, such as O–H···N.

Meanwhile, ^{1}H NMR spectra of [EtOHmim]X before and after absorption of NH_3 were further studied. First, by comparing the ^{1}H NMR spectra of [Emim][NTf_2] and [EtOHmim][NTf_2] (seeing ESI Fig. S5†), the peak at 5.16 ppm is confirmed to be the shift of H_{11} atom on the hydroxyl. Fig. 12 indicates the peak at 5.16 ppm disappears after NH_3 absorption and reappears after desorption. And the same phenomenon is also happened in the other functionalized ILs. That shows the shift of the H_{11} on hydroxyl may be dramatically affected due to the strong interaction between the electronegative N atom of NH_3 and H_{11} of hydroxyl.

The interaction between hydroxyl-functionalized cation and NH_3 molecule was further studied by the quantum chemistry

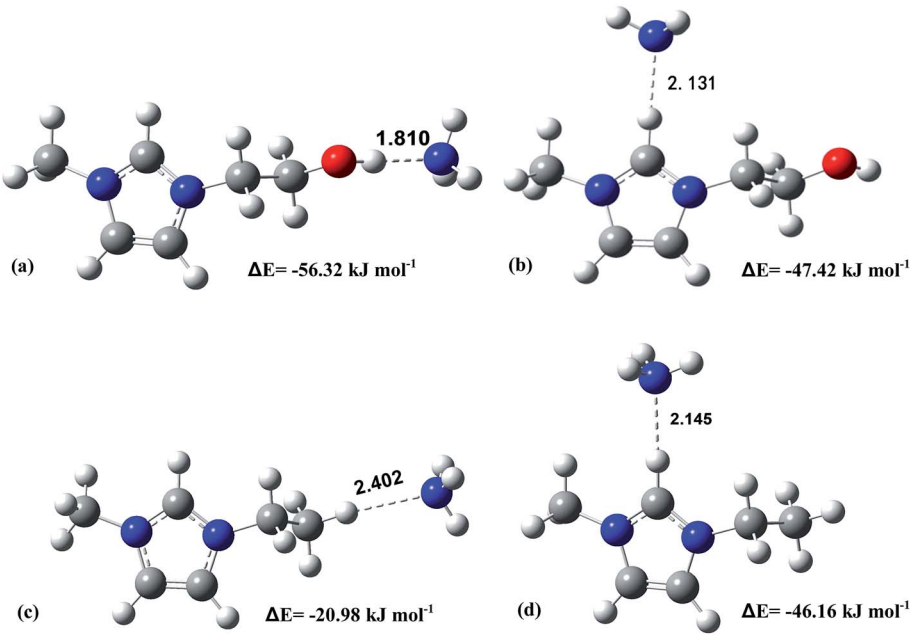

Fig. 13 Optimized structures and interaction energies for [EtOHmim]$^+$–NH_3 (a and b) and [Emim]$^+$–NH_3 (c and d) systems. O, red; N, blue; H, white; N, gray. Hydrogen bonds are indicated by dotted lines, and distances are in angstroms.

calculations at the B3LYP/6-311++G** level with Gaussian 09 software. By comparing $[EtOHmim]^+$–NH_3 system with $[Emim]^+$–NH_3 system, it can be found both the hydrogen bonding and interaction energy of $[EtOHmim]^+$–NH_3 system are stronger than those of $[Emim]^+$–NH_3 system. First, two representative structures of [EtOHmim] cation and NH_3 have been calculated. One is NH_3 located around H_{11} atom, the other is NH_3 located around H_1 atom. The optimized structures are shown in Fig. 13a and b and they are different from those in Shi's work.[27] It can be found that the hydrogen bonding is formed between N atom of NH_3 and H_{11} with distance of 1.810 Å, and the relative interaction energy is -56.32 kJ mol^{-1}. Similarly, the hydrogen bonding also can be formed between the N atom of NH_3 and H_1 with a distance of 2.131 Å, and the interaction energy is -47.42 kJ mol^{-1}. The shorter bonding length and higher interaction energy show that NH_3 prefers to interact with the H_{11} atom of hydroxyl than H_1 atom for [EtOHmim] cation and NH_3 system. For comparison, the same calculation method is used for [Emim] cation and NH_3 system. The structures are shown in Fig. 13c and d. The interaction energy between NH_3 and [Emim] cation around H_1 atom is -46.16 kJ mol^{-1}, while that around H_1 is only -20.98 kJ mol^{-1}. What's more, the hydrogen bonding length between H_1 and the N atom of NH_3 (2.145 Å) is shorter than that between H_{11} and the N atom of NH_3 (2.402 Å). The results show that NH_3 is more inclined to interact with H_1 atom of imidazole ring rather than H_{11} of C_2H_5 group for [Emim] cation and NH_3 system. By the comparison of the two systems, the higher NH_3 absorption capacity of hydroxyl-functionalized ILs than that of conventional imidazolium ILs should be attributed to the strong hydrogen bonding and interaction energy.

4. Conclusion

A series of hydroxyl-functionalized imidazolium ILs were synthesized and their physical properties as well as NH_3 absorption performance were systematically investigated. Compared with the conventional imidazolium ILs, the introducing of hydroxyl group results into the slight increase of viscosity, good thermal stability and improved NH_3 absorption capacity. Among these ILs, $[EtOHmim][NTf_2]$ has the highest NH_3 solubility, the mole fraction is 0.56 at 298.15 K and 159 kPa. The absorption cyclic experiments suggest these ILs can be regenerated. Furthermore, the absorption mechanism was detailedly studied by spectra analysis and quantum chemical calculations. The results demonstrate the excellent NH_3 absorption ability of these novel ILs is due to the strong hydrogen bonding between the N atom of NH_3 and the H atom of the hydroxyl on cation. Owing to the efficient absorption performance, simple preparation, good recyclability and excellent thermal stability, these hydroxyl-functionalized ILs could be promising candidates for NH_3 recovery.

Acknowledgements

The authors would like to acknowledge the National Basic Research Program of China (No. 2014CB744306), the National Natural Science Fund for Distinguished Young Scholars (No. 21425625), the Key Program of National Natural Science Foundation of China (21436010), and the Science and Technology Innovation Team of Cross and Cooperation of Chinese Academy of Sciences.

References

1 J. W. Erisman, A. Bleeker, J. Galloway and M. S. Sutton, *Environ. Pollut.*, 2007, **150**, 140–149.
2 C. Maton, N. D. Vos and C. V. Stevens, *Chem. Soc. Rev.*, 2013, **42**, 5963–5977.
3 C. P. Fredlake, J. M. Crosthwaite, D. G. Hert, S. N. Aki and J. F. Brennecke, *J. Chem. Eng. Data*, 2004, **49**, 954–964.
4 C. N. Dai, W. J. Wei, Z. G. Lei, C. X. Li and B. H. Chen, *Fluid Phase Equilib.*, 2015, **391**, 9–17.
5 H. S. Gao, S. J. Zeng, X. M. Liu, Y. Nie, X. P. Zhang and S. J. Zhang, *RSC Adv.*, 2015, **5**, 30234–30238.
6 A. H. Jalili, M. Shokouhi, G. Maurer and M. Hosseini-Jenab, *J. Chem. Thermodyn.*, 2014, **74**, 286.
7 J. L. Anderson, K. D. Janeille and F. B. Joan, *Acc. Chem. Res.*, 2007, **40**, 1208–1216.
8 T. Nonthanasin, A. Henni and C. Saiwan, *RSC Adv.*, 2014, **4**, 7566.
9 M. Ramdin, S. P. Balaji, J. Manuel Vicent-Luna, J. J. Gutierrez-Sevillano, S. Calero, T. W. de Loos and T. J. H. Vlugt, *J. Phys. Chem. C*, 2014, **118**, 23599–23604.
10 L. C. Tome, M. Isik, C. S. R. Freire, D. Mecerreyes and I. M. Marrucho, *J. Membr. Sci.*, 2015, **483**, 155–165.
11 Z. Z. Yang, Y. N. Zhao and L. N. He, *RSC Adv.*, 2011, **1**, 545.
12 P. J. Carvalho and J. A. P. Coutinho, *Energy Fuels*, 2010, **24**, 6662–6666.
13 G. K. Cui, W. J. Lin, F. Ding, X. Y. Luo, X. He, H. R. Li and C. M. Wang, *Green Chem.*, 2014, **16**, 1211–1216.
14 G. K. Cui, C. M. Wang, J. J. Zheng, Y. Guo, X. Y. Luo and H. R. Li, *Chem. Commun.*, 2012, **48**, 2633–2635.
15 S. Y. Sun, Y. X. Niu, Q. Xu, Z. Sun and X. H. Wei, *RSC Adv.*, 2015, **5**, 46564–46567.
16 Z. Z. Yang, L. N. He, Q. W. Song, K. H. Chen, A. H. Liu and X. M. Liu, *Phys. Chem. Chem. Phys.*, 2012, **14**, 15832–15839.
17 S. J. Zeng, H. Y. He, H. S. Gao, X. P. Zhang, J. Wang, Y. Huang and S. J. Zhang, *RSC Adv.*, 2015, **5**, 2470–2478.
18 S. J. Zeng, H. Y. He, H. S. Gao and X. P. Zhang, *RSC Adv.*, 2015, **5**, 2470–2478.
19 Y. Zhao and G. X. Hu, *RSC Adv.*, 2013, **3**, 2234–2240.
20 M. A. Ahmadi, R. Haghbakhsh, R. Soleimani and M. B. Bajestani, *J. Supercrit. Fluids*, 2014, **92**, 60–69.
21 C. A. Faundez, J. F. Diaz-Valdes and J. O. Valderrama, *Fluid Phase Equilib.*, 2014, **375**, 152–160.
22 K. Huang, Y. L. Chen, X. M. Zhang, S. L. Ma, Y. T. Wu and X. B. Hu, *Fluid Phase Equilib.*, 2014, **378**, 21–33.
23 Y. Q. Ma and R. Wang, *Chem. Res. Chin. Univ.*, 2014, **35**, 1515–1522.
24 A. Yokozeki and B. S. Mark, *Ind. Eng. Chem. Res.*, 2007, **46**, 1605–1610.
25 A. Yokozeki and M. B. Shiflett, *Appl. Energy*, 2007, **84**, 1258–1273.

26 G. H. Li, Q. Zhou, X. P. Zhang, L. Wang, S. J. Zhang and J. W. Li, *Fluid Phase Equilib.*, 2010, **297**, 34–39.
27 W. Shi and E. J. Maginn, *AIChE J.*, 2009, **55**, 2414–2421.
28 J. Palomar, G. Miquel-Maria, J. Bedia, F. Rodriguez and J. J. Rodriguez, *Sep. Purif. Technol.*, 2011, **82**, 43–52.
29 S. K. Tang, G. A. Baker and H. Zhao, *Chem. Soc. Rev.*, 2012, **41**, 4030–4066.
30 J. Z. Zhang, C. Jia, H. F. Dong, J. Q. Wang, X. P. Zhang and S. J. Zhang, *Ind. Eng. Chem. Res.*, 2013, **52**, 5835–5841.
31 M. Zhu, M. X. Zhu, Y. Song, W. Z. Liang, W. Han and Y. N. Chen, *Engineering and manufacturing technologies*, 2014, **541–542**, 78–82.
32 P. Brown, B. E. Gurkan and T. A. Hatton, *AIChE J.*, 2015, **61**, 2280–2285.
33 L. J. Wazer JRV, K. Y. Kim and R. E. Colwell, *Viscosity and Flow Measurement*, New York: Wiley, 1963, 406.
34 P. Navarro, M. Larriba, E. Rojo, J. García and F. Rodríguez, *J. Chem. Eng. Data*, 2013, **58**, 2187–2193.